COMPARISON OF FREQUENCY-BAND SELECTION STRATEGIES FOR 2D TIME-DOMAIN ACOUSTIC WAVEFORM INVERSION

XIAONA MA[1,2], ZHIYUAN LI[1], SHANHUI XU[1], PEI KE[3] and GUANGHE LIANG[1]

[1] *Key Laboratory of Mineral Resources, Institute of Geology and Geophysics, Chinese Academy of Sciences, Beijing 100029, P.R. China. maxiaona@mail.iggcas.ac.cn*
[2] *University of Chinese Academy of Sciences, Beijing 100049, P.R. China.*
[3] *BGP Inc., China National Petroleum Corporation, Hebei Zhuozhou 072751, P.R. China.*

(Received January 13, 2017; revised version accepted October 3, 2017)

ABSTRACT

Ma, X., Li, Z., Xu, S., Ke, P. and Liang, G., 2017. Comparison of frequency-band selection strategies for 2D time domain acoustic waveform inversion. *Journal of Seismic Exploration*, 26: 499-519.

Full waveform inversion (FWI) is a promising model-building technology to recover subsurface information. However, it is easy to fall into local minima when applying this method because of the lack of a low-frequency component in seismic data. To mitigate this problem, multi-scale method for the time domain has been proposed. With this method, we perform the inversion sequentially from low- to high-frequency groups, and we set the velocity model inverted at the previous scale as an initial velocity model for the next higher frequency group. In this study, we mainly compare several frequency-band selection strategies for FWI in time domain, including individual-grouping methods 1 and 2, along with Bunks' method. To verify and compare the efficiency of the above three methods, we introduce the partial-overlap and arbitrary-two grouping methods. Numerical examples for synthetic data of the Marmousi velocity model, as well as noisy data, demonstrate that multiscale inversion can attain encouraging resolution. Compared to solutions from other methods, we highlight the individual-grouping method 2 which can yield a more satisfactory velocity model. Also, numerical results imply that low frequencies are necessary in full waveform inversion.

KEY WORDS: full waveform inversion, time-domain multiscale method, frequency-band selection strategies

0963-0651/17/$5.00

INTRODUCTION

Full waveform inversion (FWI) as a method of building high-precision subsurface structures has been studied for decades. Lailly (1983) and Tarantola (1984) first proposed a back-propagation technique for waveform inversion, and many evolved approaches to waveform inversion algorithms have since appeared (Min et al., 2015). It can be implemented in the time domain (Tarantola, 1984; Gauthier et al., 1986; Mora, 1987), frequency domain (Pratt et al., 1998; Plessix, 2006; Shin and Min, 2006), or Laplace domain (Shin and Cha, 2008; 2009).

In the frequency domain, FWI uses an implicit finite-difference technique for frequency-space modeling. It is efficient to implement parallel applications for a larger number of shots, but it imposes huge memory requirements, making this method more applicable to 2D or smaller 3D problems (Liu, 2015; Operto et al., 2007a). In the time domain, we can apply higher-order finite-difference schemes for numerical simulations to maintain high accuracy, and it occupies less memory, which is suitable for solving large 3D problems. In general, FWI is always solved iteratively using local optimization methods, such as the preconditioned conjugate-gradient method and limited-memory Broyden-Fletcher-Goldfarb-Shanno (L-BFGS) optimization method, which gradually minimizes the waveform differences between calculated and observed data (Virieux and Operto, 2009). Global optimization methods have also been used to obtain the optimal solution, but they are rarely applied to practical problems due to the huge calculation burden.

Though FWI can theoretically construct well-resolved velocity structures, there exists a critical problem. Since the relationship between observed field data and model parameters is always strongly nonlinear, if the starting model is far from the global minimum, the waveform inversion is likely to get trapped into a local minimum (Gauthier et al., 1986). And seismic data always lack low-frequency information, which will result in seismic inversions with poor sensitivity to the long and intermediate wavelengths (Symes, 2008; Ha and Shin, 2012).

Some efforts have been made in recent years to overcome the problem of local minima. Early studies tried to linearize the relationship between observed field data and model parameters (Tarantola, 1984; Berkhout, 1984), but this method only works when the initial model is close to the true model (Kim et al., 2010). Some researchers sought a better initial model for FWI by employing traveltime tomography (Brenders and Pratt, 2007; Gao et al., 2007; Biondi and Almomin, 2013) or migration velocity analysis (Symes, 2008). Other investigators have tried to use low-frequency components by acquiring wide azimuth data (Ravaut, et al., 2004). As an efficient selection, a multiscale waveform inversion method has been proposed, aiming toward full waveform inversion in the time-domain (Bunks et al., 1995) and successive inversion of single frequencies in the frequency domain (Pratt, 1999). So far, the multiscale methods have been applied widely in a full waveform inversion scheme.

As is well known, the multiscale approach is a natural benefit for frequency-domain inversion, due to seismic data that have already been decomposed into separate frequency components using the Fourier transform (Brenders and Pratt, 2007). Sirgue (2004) presented a practical strategy of selecting frequencies for frequency-domain inversion, which takes advantage of wavenumber redundancy. Anagaw and Sacchi (2014) made comparisons of six frequency selection strategies for FWI in frequency domain; and proposed that partially overlapped groups of temporal frequencies can obtain better resolution for the velocity models than the other methods. However, for the time domain, all frequencies are inverted simultaneously, which makes it easy to fall into local minima. To solve such a problem, Bunks (1995) proposed the multigrid method that uses several frequency bands of data and varying grid sizes to obtain satisfactory results in the time domain. Seismic data and the source are low-pass filtered to different cutoff frequencies of interest using Hamming-window function, but high-frequency component leakage may exist. Boonyasiriwat et al. (2009) modified the multi-grid method and proposed a new strategy for choosing optimal frequency bands based on wavenumber continuity. At the same time, a Wiener filtering function has proved efficient to filter the data. Liu (2015) proposed a new frequency-band choosing strategy from the relation between peak frequencies, and it is simple to calculate the frequency-band used in FWI. Aiming to find a better multiscale strategy for FWI in the time domain, we compare the different frequency selection strategies and provide numerical examples in this study.

This paper is divided into five sections. After the introduction, we describe the theory of full waveform inversion for the time domain, and we present the Wiener window function for frequency-band filtering. Then we study and compare frequency-band selection strategies in the time domain. In the fourth section, we provide numerical examples using six different strategies for the Marmousi model. We present our conclusions in the last section.

REVIEW OF FULL WAVEFORM INVERSION IN TIME DOMAIN

The 2D acoustic wave equation is

$$\frac{1}{v(\mathbf{x})^2}\frac{\partial^2 p(\mathbf{x},t)}{\partial t^2}=\left[\frac{\partial^2 p(\mathbf{x},t)}{\partial x^2}+\frac{\partial^2 p(\mathbf{x},t)}{\partial z^2}\right]+s(\mathbf{x},t) \quad , \qquad (1)$$

where $p(\mathbf{x},t)$ represents the pressure field, $v(\mathbf{x},t)$ is the acoustic velocity (representing the model $\mathbf{m}$) and $s(\mathbf{x},t)$ is a source term. The time-domain forward modeling of eq. (1) is solved by an explicit finite-difference scheme with 12th-order accuracy in space and second-order accuracy in time. In the forward modeling part, we apply the perfectly matched layer (PML) condition at boundaries (Bérenger, 1994).

In seismic inversion, the misfit function is usually constructed by a l_2 norm of residuals between field data and numerical data. So, the misfit function can be written in the time domain as

$$E = \frac{1}{2}\sum_s \sum_g \left[p^{cal}(\mathbf{x},t) - p^{obs}(\mathbf{x},t) \right]^2 \quad , \tag{2}$$

where $p^{\mathrm{cal}}(\mathbf{x},t)$ and $p^{\mathrm{obs}}(\mathbf{x},t)$ are the calculated and observed data, respectively. The primary purpose of FWI is to minimize misfit function (2), so that we obtain the optimal velocity model. In this paper, we apply the L-BFGS optimization method to minimize the misfit function (Nocedal and Wright, 2006). The gradient of the misfit function can be obtained by calculating the partial derivative of eq. (2) with respect to the velocity model, which can be expressed as the zero-lag value of the cross-correlations between the forward-propagated wavefield and the back-propagated wavefield residuals (Plessix, 2006):

$$g = \frac{\partial E}{\partial m} = \frac{2}{v(x)^3}\int_0^T \lambda \frac{\partial^2 p(\mathbf{x},t)}{\partial t^2} dt \quad , \tag{3}$$

where T represents the maximum time record, and λ represents the back-propagated residual wavefield. It is obtained by back-propagating the residual wavefield, which can be defined as

$$\delta p = \sum_g p^{cal}(\mathbf{x},t) - p^{obs}(\mathbf{x},t) \quad . \tag{4}$$

The model can be updated by using the relationship

$$\mathbf{m}_{k+1} = \mathbf{m}_k + \alpha_k d_k \quad , \tag{5}$$

where $\mathbf{m}_{k+1}$ and $\mathbf{m}_k$ represent the (k+1)-*th* and k-*th* iteration model parameter, respectively. The variable α_k represents the step length, whose role can be regarded as converting the units of the gradient vector to model dimensions (Pratt, 1998). The step length is determined by the backtracking line search method combined with the first Wolfe condition (Nocedal and Wright, 2006). For FWI, the source wavelet is probably known or estimated with the initial model before inversion (Shin and Cha, 2008, 2009).

LOW-PASS FILTERING AND FREQUENCY-BAND SELECTION STRATEGIES

In conventional waveform inversion in the time-domain, multiple frequencies for a given broad bandwidth are inverted simultaneously, and they usually fall into local minima. Now, with the multiscale method, FWI can obtain encouraging results in the time domain. It needs to decompose the seismic data into several frequency band groups, then perform sequentially from low to high frequencies. Therefore, in this scheme, low-pass filtering and frequency-band selection strategies are two essential factors to successful multiscale inversion.

Low-pass filtering

There are many filter functions, such as Hamming, Wiener and Blackman-Harris window functions. Compared to the Hamming-window function, the Wiener and Blackman-Harris window functions have minimal high-frequency component leakage (Boonyasiriwat et al., 2009). The Wiener filter can be computed as

$$f_{Wiener}(\omega) = \frac{W_{target}(\omega) W^{*}_{original}}{\left|W_{original}(\omega)\right|^{2} + \varepsilon^{2}} \quad , \tag{6}$$

where f_{Wiener} is the Wiener filter, $W_{original}$ the original wavelet, W_{target} is the low-frequency target wavelet, ω is the angular frequency, ε is a small parameter that prevents numerical overflow, and $*$ denotes the complex conjugate. As illustrated in Fig. 1, Wiener filtering can obtain a wavelet with a user-selected low-frequency band.

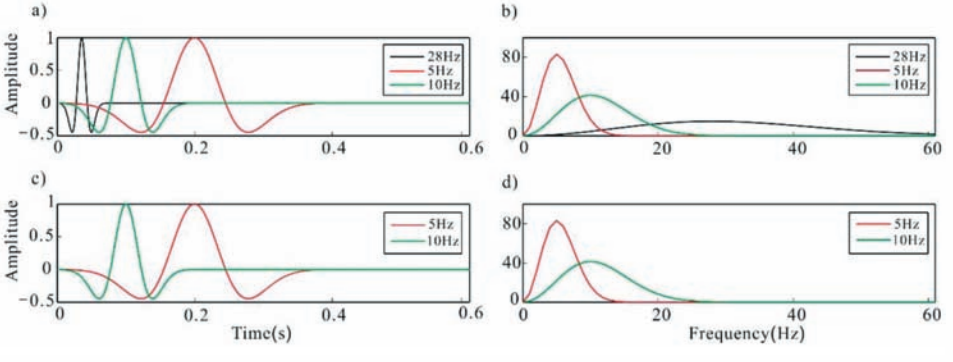

Fig. 1. a) Original 28-Hz (black), 10-Hz (green), and 5-Hz (red) Ricker wavelet. b) Amplitude spectrum corresponding to wavelet in a). c) 10-Hz (green) and 5-Hz (red) Ricker wavelet low-pass filtered by Wiener filter from 28-Hz Ricker wavelet. d) Amplitude spectrum corresponding to wavelet in c).

To validate the efficiency of a filtering function on observed data, we implement it on the synthetic seismograms generated with both 25-Hz [Fig.2(a)] and 6.9-Hz [Fig. 2(c)] Ricker wavelets for a 2D model. We transform the 25-Hz seismograms into 6.9-Hz seismograms [Fig. 2(b)] and compare them with original seismograms simulated with a 6.9-Hz Ricker wavelet [Fig. 2(c)]. For detailed comparisons, we also extract arbitrary traces (Fig. 3) from seismograms in Fig. 2. By observation, we see that the Wiener filter is efficient for filtering synthetic seismograms to obtain the low frequency bands we are interested in. The minimal spectral leakage at the beginning and end of traces, shown in Fig. 3, may be caused by truncation of data.

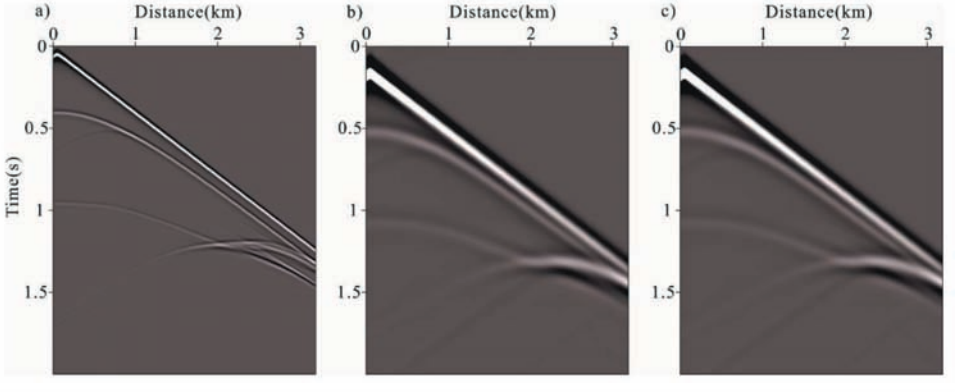

Fig. 2. a) Original unfiltered synthetic seismograms of 2D model generated from a 25-Hz Ricker wavelet. b) Synthetic seismograms low-pass filtered by the Wiener filter to the frequency band of a 6.9-Hz Ricker wavelet. c) Original synthetic seismograms of 2D model generated from a 6.9-Hz Ricker wavelet.

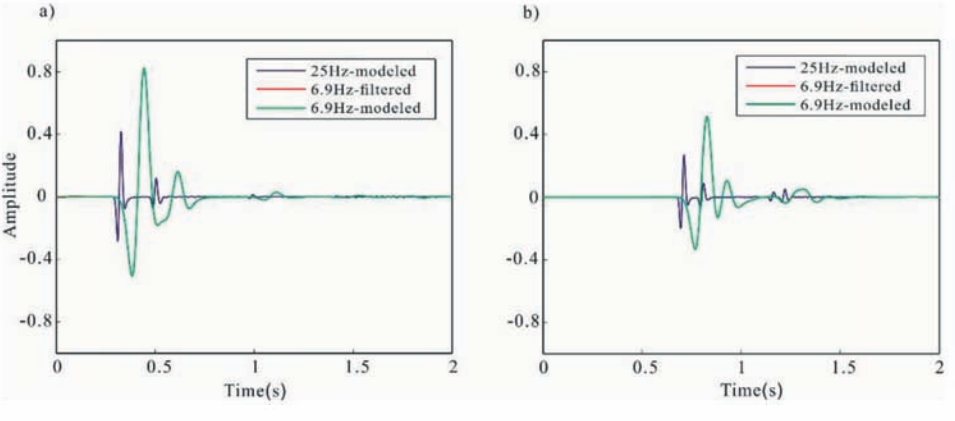

Fig. 3. a) Traces corresponding to Fig. 2 at a horizontal position of 0.8 km. b) Traces corresponding to Fig. 2 at a horizontal position of 1.8 km.

To test Wiener filtering in more realistic conditions, we contaminate synthetic data (Fig. 2) with random noise with a signal-to-noise ratio (S/N) of 32 dB (Fig. 4). It can be seen that random noise will cause filtered results to deviate from the original, especially at both ends of the data (Fig. 5).

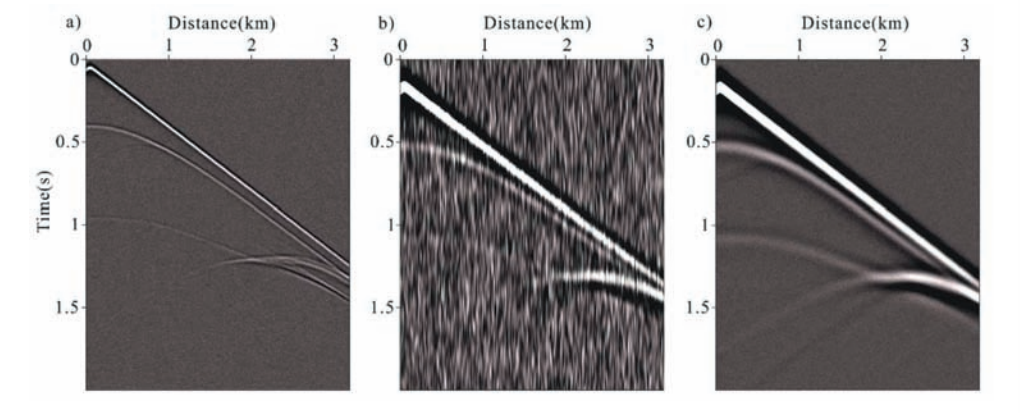

Fig. 4. a) Original unfiltered synthetic seismograms of 2D model generated from a 25-Hz Ricker source wavelet, adding random noise, 32 dB. b) Synthetic seismograms low-pass filtered by the Wiener filter to the frequency band of a 6.9-Hz Ricker wavelet. c) Original synthetic seismograms of 2D model generated from a 6.9-Hz Ricker source wavelet, adding random noise, 32 dB.

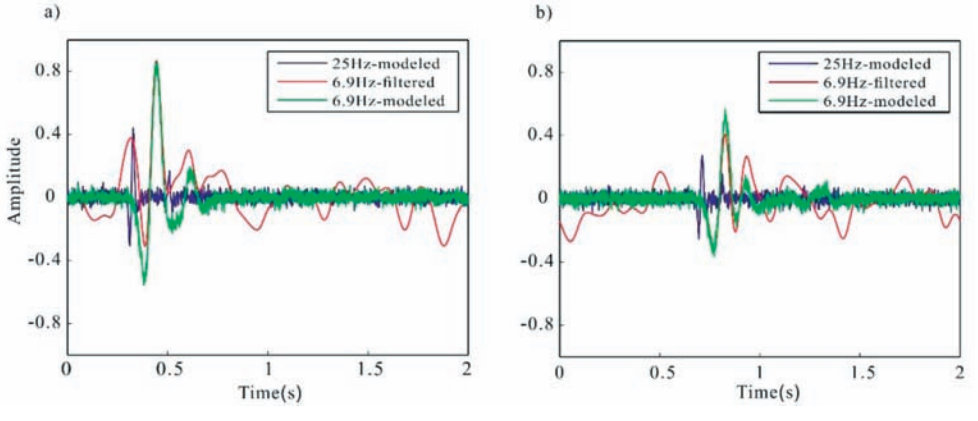

Fig. 5. a) Traces corresponding to Fig. 4 at a horizontal position of 0.8 km. b) Traces corresponding to Fig. 4 at a horizontal position of 1.8 km.

Frequency-band selection strategies

Regarding the local-minima problem, Bunks (1995) proposed a multigrid strategy that decomposed inversion into several scales, performed sequentially over frequency groups in inversion, and repeatedly used low frequencies at every stage. We usually begin by low-pass filtering data, and then broaden the frequency ranges toward high frequencies. The velocity model inverted at the previous scale is set as the initial model for next scale. We can achieve greater computational efficiency at low frequencies by computing numerical solutions of the wave equation using coarser grids and larger time sampling intervals than at high frequencies. And no matter how the sampling time *dt* and the grid dimensions *dx* and *dz* change, we must maintain numerical stability. Fig. 6 shows the flow chart of multiscale full waveform inversion using the frequency-band selection criterion.

We can achieve greater computational efficiency at low frequencies by computing numerical solutions of the wave equation using coarser grids and larger time sampling intervals than at high frequencies. And no matter how the sampling time *dt* and the grid dimensions *dx* and *dz* change, we must maintain numerical stability. Fig. 6 shows the flow chart of multiscale full waveform inversion using the frequency-band selection criterion.

Individual-grouping method 1

In the frequency domain, Sirgue (2004) proposed that each frequency had a limited and finite band contribution to the image spectrum. For a given frequency, the wavenumber coverage is limited to the range $[k_{z\min},k_{z\max}]$ where $k_{z\min}$ and $k_{z\max}$ are calculated as follows:

$$\begin{cases} k_{z\min} = 4\pi f \alpha_{\min} / c_0 \\ k_{z\max} = 4\pi f / c_0 \end{cases}, \quad \text{with} \quad \alpha_{\min} = \frac{1}{\sqrt{1+R_{\max}^2}}, \tag{7}$$

where $R_{\max} = h_{\max}/z$, $h_{\max}$ represents the maximum half offset, and z represents the depth of target structure. When we select an inversion frequency, we need to maintain wavenumber continuity, i.e.,

$$k_{z\min}\left(f_{n+1}\right) = k_{z\max}\left(f_n\right), \tag{8}$$

Therefore, we can obtain the inversion frequency by following the relation (Fig. 7)

$$f_{n+1} = \frac{f_n}{\alpha_{\min}}, \tag{9}$$

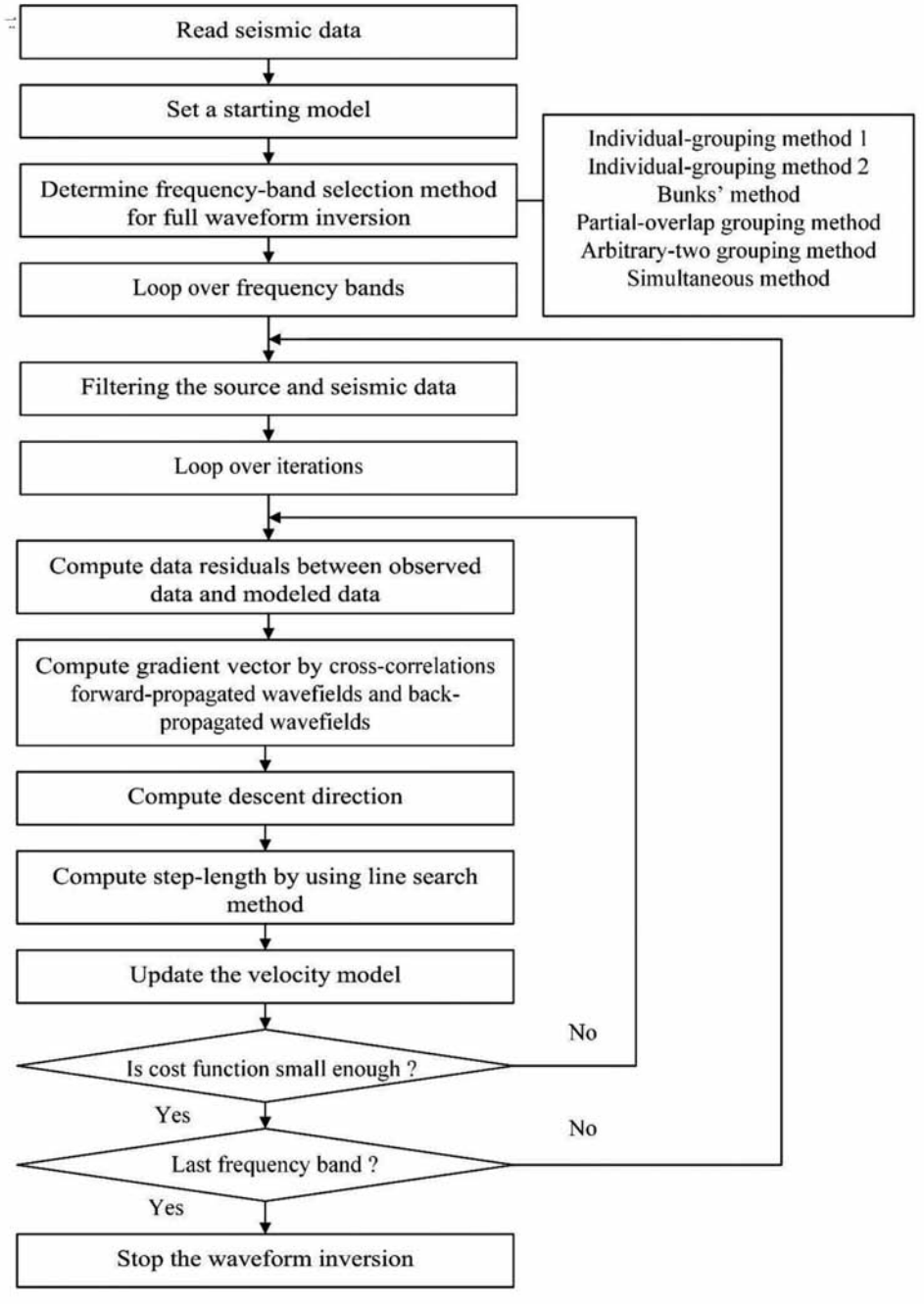

Fig. 6. Flowchart of multiscale full waveform inversion in time domain.

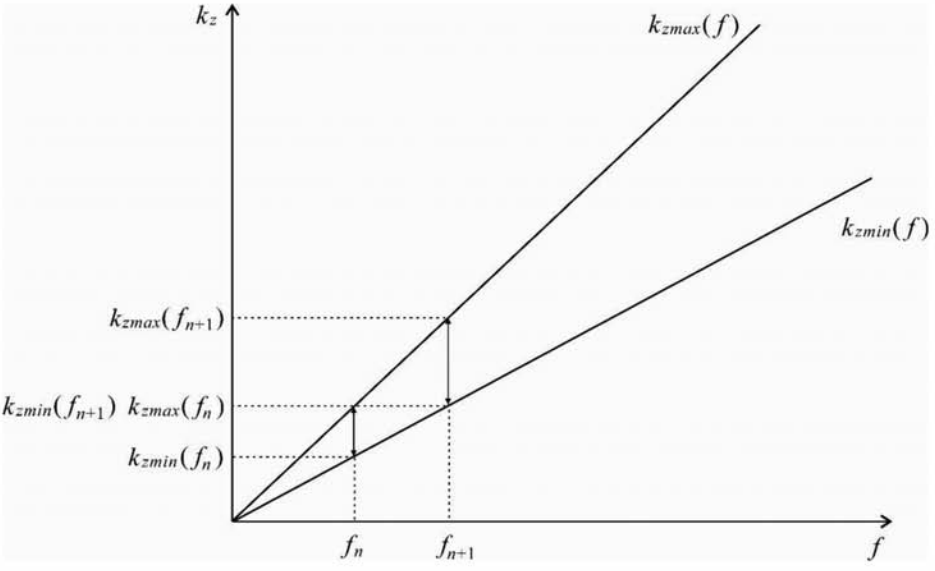

Fig. 7. Strategy of selecting inversion frequency in frequency domain based on wavenumber continuation.

In this paper, in the n-th frequency band, the minimum and maximum frequencies of the band determine the wavenumber range, whose minimum and maximum values are respectively defined as follows (Fig. 8):

$$\begin{cases} k_{z\min}(n) = \dfrac{4\pi f_{\min}(n)\alpha_{\min}}{c_0}, \\ k_{z\max} = \dfrac{4\pi f_{\max}(n)}{c_0}. \end{cases} \quad . \tag{10}$$

In a similar way to the frequency domain, we define

$$k_{z\min}(n+1) = k_{z\max}(n) \quad . \tag{11}$$

Therefore, we can obtain the following frequency relation between different frequency bands:

$$f_{\min}(n+1) = \frac{f_{\max}(n)}{\alpha_{\min}} \quad , \tag{12}$$

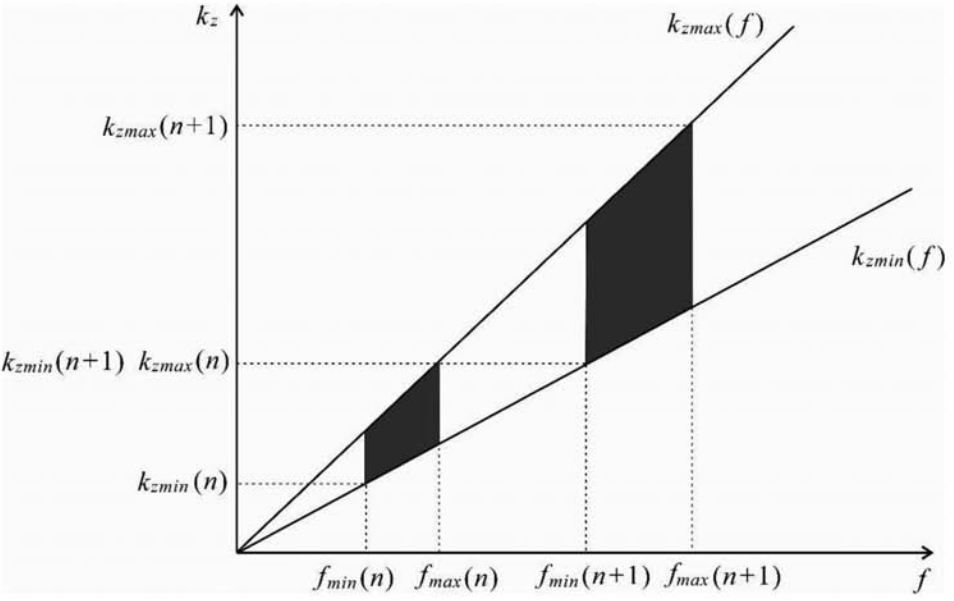

Fig. 8. Strategy of selecting inversion frequency band in time domain based on wavenumber continuation.

For the first scale, we set the frequency at half the maximum spectral amplitude at the left end as the minimum frequency, and we set the frequency at half the maximum spectral amplitude at the right end as the maximum frequency. For the second scale, we use eq. (12) to calculate $f_{\min}(2)$, and $f_{\max}(2) = f_{\min}(2) + f_{\text{band}}$, where f_{band} represents the width of the frequency-band. We use an analogous relationship for the next scale, so wavenumber coverage is complete and continuous, with no overlap.

Individual-grouping method 2

Here, we present a new frequency-band choosing strategy, which is determined as follows. We first confirm the peak frequency using the equation:

$$f(j-1) = \beta f(j) \quad (j = 1, nscale) \ , \tag{13}$$

where *nscale* represents the decomposed scale, *f(nscale)* represents the peak frequency, and β is a coefficient with value range $[0.2 \sim 0.3]$. Then, with respect to the first scale, we set the minimum frequency at half the maximum spectral amplitude at the left end, and we set the maximum frequency at half the maximum spectral amplitude at the right end.

NUMERICAL EXAMPLES

In this section, we check the feasibility of the frequency-band selection methods presented in this paper. As is well known, the Marmousi velocity model (Fig. 9) has a complicated structure and a high-velocity layer at a depth of about 1.5 km, and it is not easy to image the anticline structure below the high-velocity layer (Kim, 2011).

In all experiments, we use two criteria to make the iteration process terminate. The first one states that the iteration number must not exceed an adequate maximum value at each stage. The second one states that the inversion process will stop if the objective function value increases or the relative change of the objective function value is less than a minimal value. Besides that, the implementation algorithms of FWI are identical, except for different frequency band selection strategies.

Marmousi velocity model

We resize the modified Marmousi velocity model to 361×142 samples, with an interval of 12-m in each direction. The true velocity model is shown in Fig. 9(a), and we create the initial velocity model by a linear function of depth, as shown in Fig. 9(b). We create synthetic data using the time-domain, finite-difference method, with 36 shots and 360 geophones, which are distributed along the surface in the horizontal direction. The source signal is a Ricker wavelet with a peak frequency of 22 Hz. Table 1 shows the frequency bands we used in this test.

Table 1. Frequency band selection strategies for full waveform inversion (Marmousi synthetic data).

Method	Frequency band (Hz)
Individual-grouping method 2	
	0.48–1.65
	2.89–9.80
	10.60–36.00
Simultaneous method	0.00–66.00

The inversion result falls into a local minimum after 35 iterations, when we use conventional FWI. Fig. 10(a) shows the conventional simultaneous inversion result. There is a huge deviation between the inversion result and the true mode, in both the shallow and deep parts. Fig. 10(b) shows the difference between the true Marmousi model and the inverted velocity model. The simultaneous inversion method performs very poorly for inverting the velocity model, which yield local minimum solutions for the simultaneous inversion.

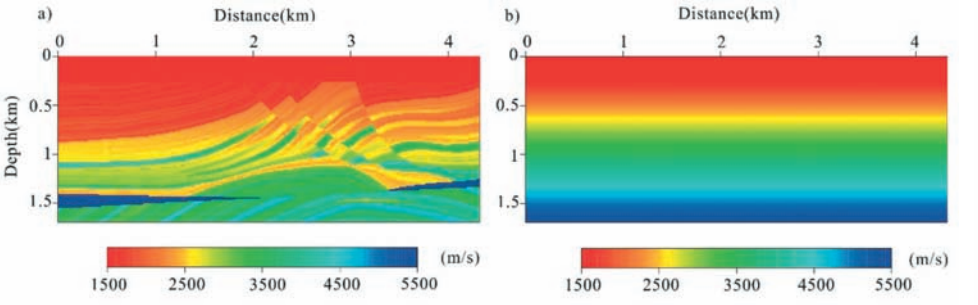

Fig. 9. a) Marmousi velocity model. b) The initial velocity model is created by a linear function of depth.

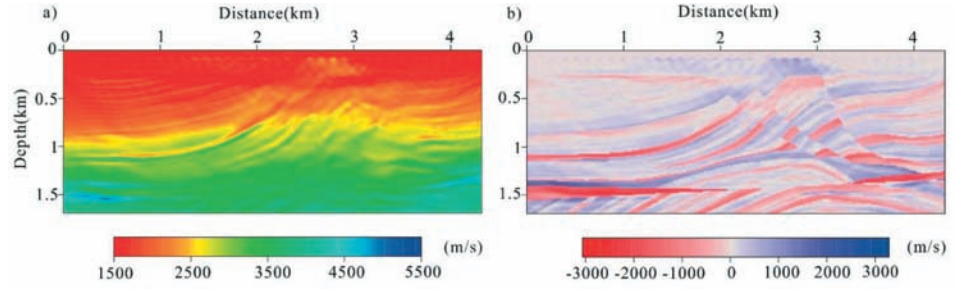

Fig. 10. a) Inversion results of the simultaneous method. b) Difference between true Marmousi model and inverted model.

Then we make use of a multiscale method, setting the velocity model obtained at the lower-frequency band as an initial model for the next frequency band. Fig. 11 shows the inverted velocity model of the three frequency bands from individual-grouping method 2; compared with the conventional FWI, the inversion accuracy has been significantly improved. It can be seen that by using the inversion process from lower frequency bands to higher frequency bands in sequence, the structures and features are recovered more and more accurately. The first scale inversion result shows that it can recover long wavelength components of model parameters from low-frequency information. Then, the second and third scales invert structures and thin layers gradually, which correspond to the intermediate and short-wavelength components.

For more detailed comparisons, we show depth-velocity profiles of the true, initial and final inverted velocity models at horizontal positions of 0.66 km, 1.86 km, and 2.34 km, respectively, in Figs. 12(a), (b), and (c). The inverted velocity profiles appear to show a trend that is similar to that of the true velocity profile. Unfortunately, due to uneven spatial distribution of seismic energy in the model, the deep region of the model is not reconstructed as well as the shallow region.

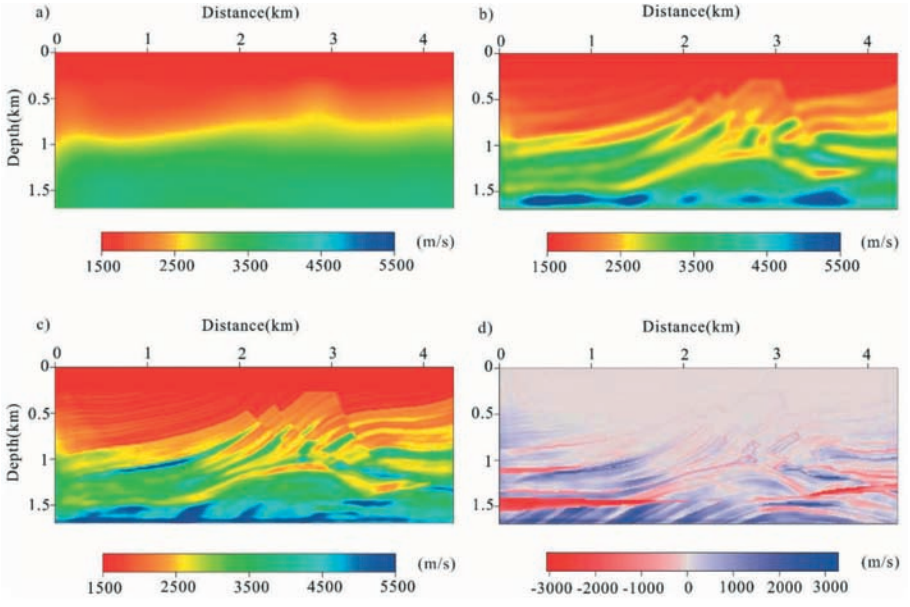

Fig. 11. a) Inverted velocity model of the first scale. b) Inverted velocity model of the second scale. c) Inverted velocity model of the third scale. d) Difference between true Marmousi model and final inverted velocity model.

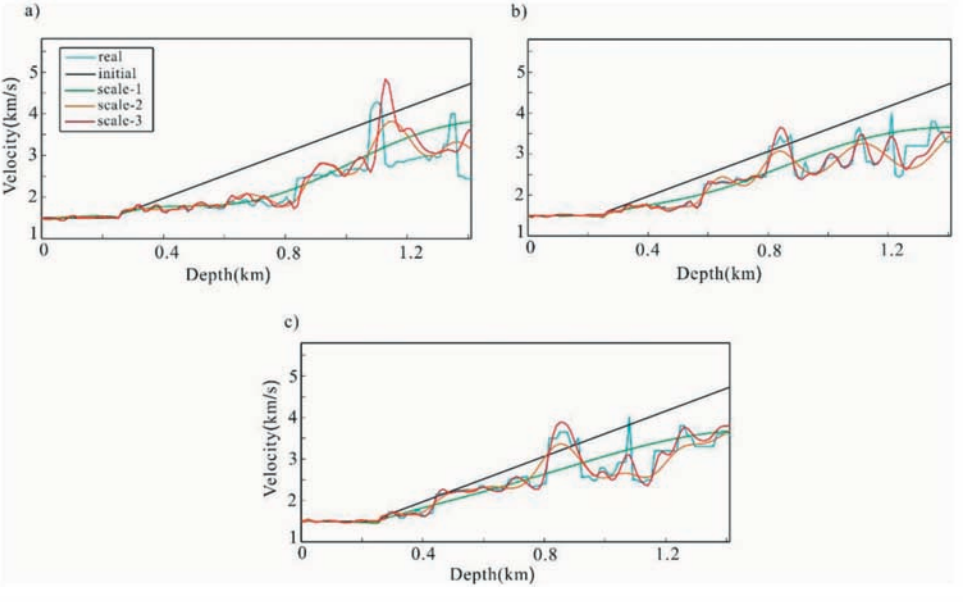

Fig. 12. a) Depth profiles of the real, initial, and final inverted velocities at a horizontal position of 0.66 km. b) Depth profiles of the real, initial, and final inverted velocities at a horizontal position of 1.86 km. c) Depth profiles of the real, initial, and final inverted velocities at a horizontal position of 2.34 km.

Marmousi velocity with random noise

To test our waveform inversion algorithm in more realistic conditions, we added random noise to synthetic data. Fig. 13 shows a synthetic seismogram contaminated with random noise with a signal-to-noise ratio (S/N) of 32 dB. Table 2 shows the frequency bands using in inversion calculated from different selection strategies.

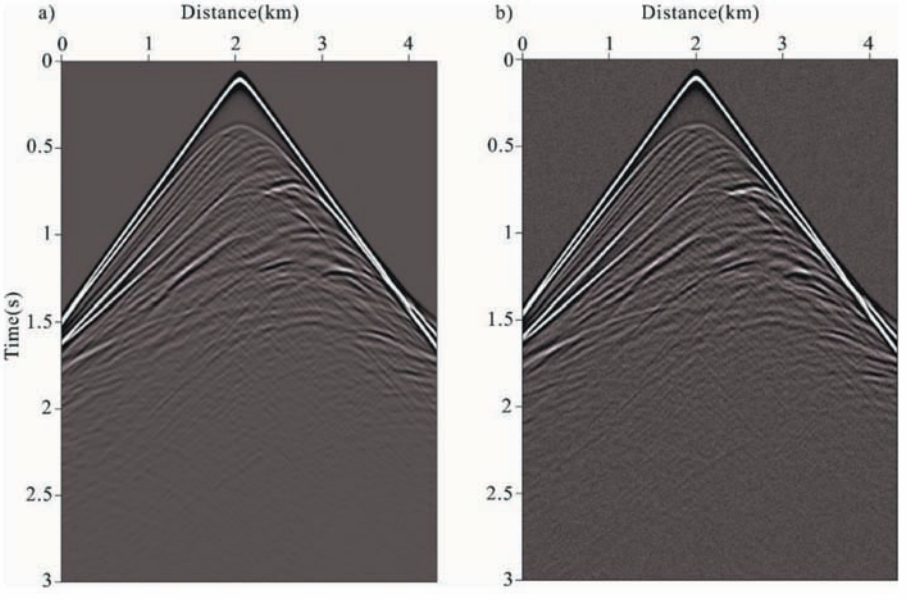

Fig. 13. a) Synthetic seismograms from true Marmousi model. b) Synthetic seismograms contaminated with noise, 32 dB.

Table 2. Frequency band selection strategies for full waveform inversion (Marmousi synthetic data contaminated with noise, 32 dB).

Method	Frequency band (Hz)
Individual-grouping method 1	0.00–3.00
	4.84–7.84
	12.65–36.00
Individual-grouping method 2	0.48–1.65
	2.89–9.80
	10.60–36.00
Bunks' Method	0.00–1.65
	0.00–9.80
	0.00–36.00
Partial-overlap grouping method	1.93–6.53
	4.33–14.70
	10.60–36.00
Arbitrary-two grouping method	2.418–8.17
	10.60–36.00
Simultaneous method	0.00–66.00

Fig. 14 depicts the final inverted velocity models from noisy data. In can be seen that Bunks' method, individual-grouping method 1 and individual-grouping method 2 outperform the other methods in terms of resolution, and that the frequency-band selection strategies enhance the feasibility for global minimum solutions. However, the partial overlap grouping method, arbitrary-two grouping method and simultaneous method are not suitable, as they may fall into local minima. This can be confirmed by computing the residuals between the true model and different inversion results. Fig. 15 depicts the absolute difference between the true Marmousi model and the inverted velocity models in Fig. 14.

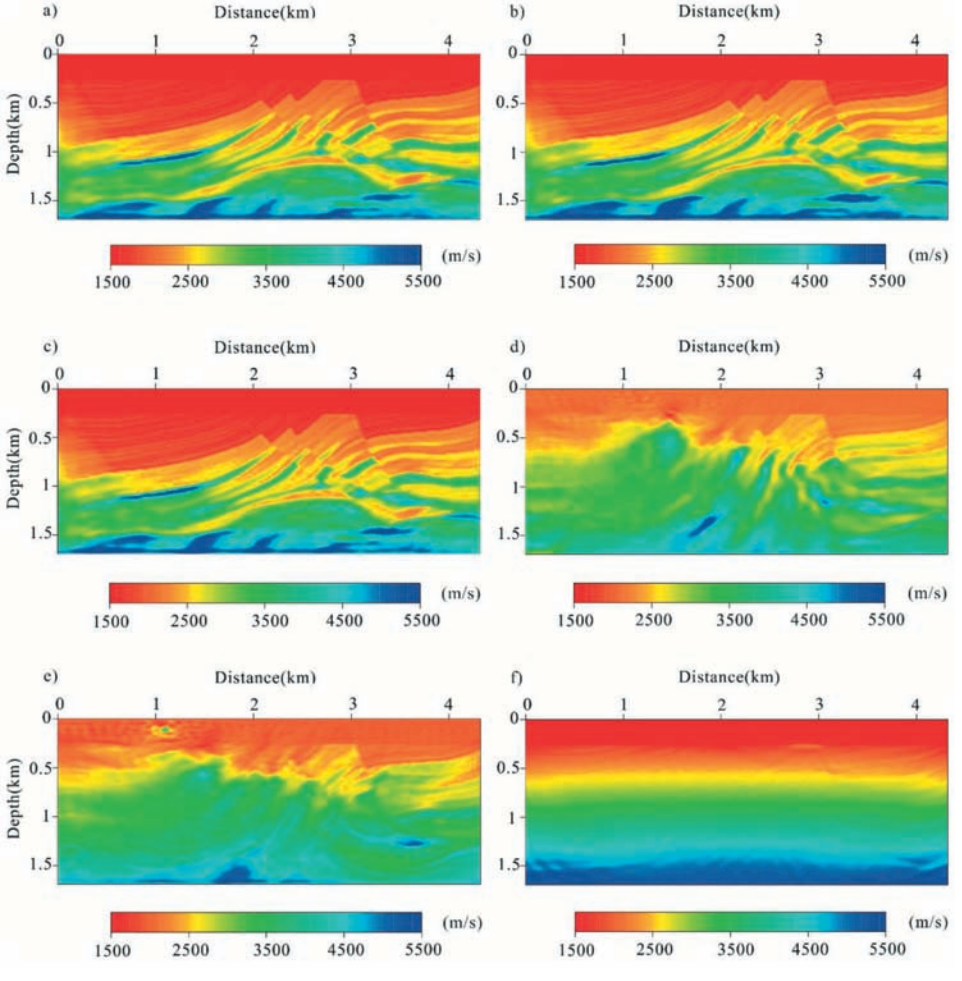

Fig. 14. Inversion results from noisy data with S/N of 32 dB using: a) individual-grouping method 1; b) individual-grouping method 2; c) Bunks' method; d) partial-overlap grouping method; e) arbitrary-two grouping method; f) simultaneous method.

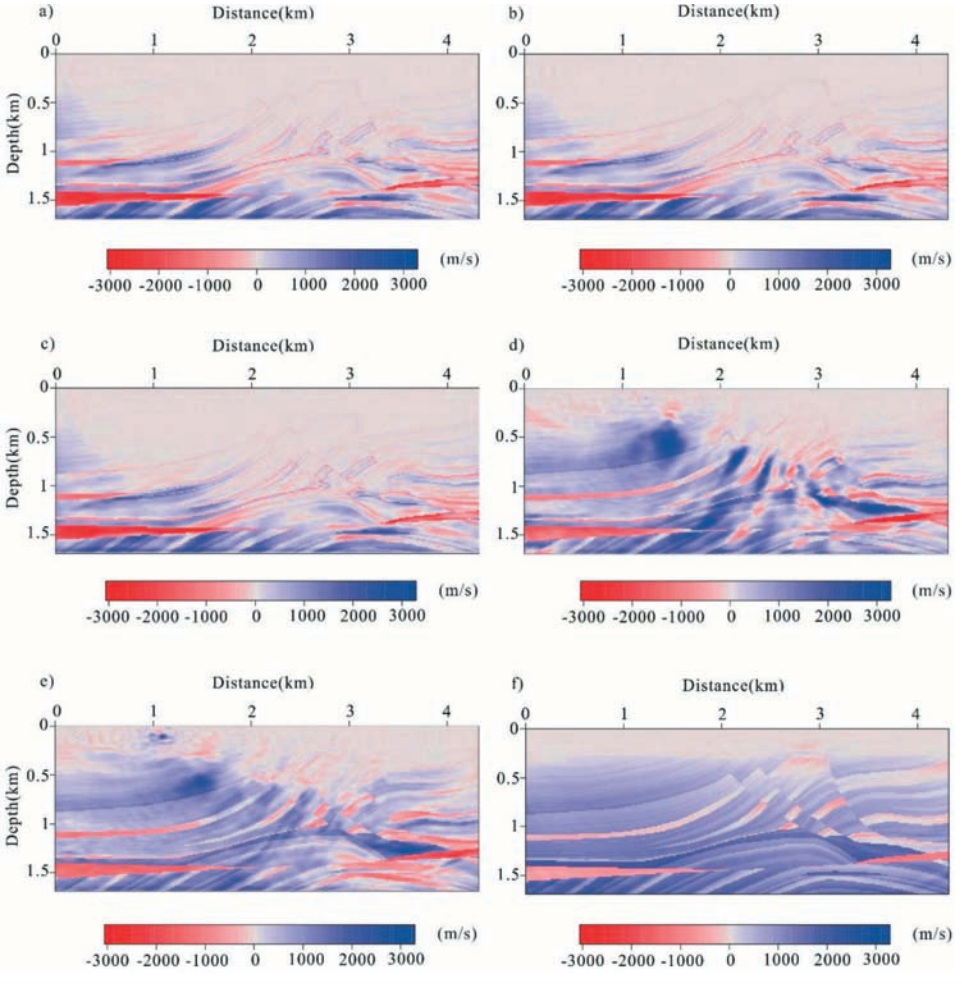

Fig. 15. Difference between true Marmousi model and final inverted velocity model in Fig. 14: the residual from the velocity model using a) individual-grouping method 1; b) individual-grouping method 2; c) Bunks' method; d) partial-overlap grouping method; e) arbitrary-two grouping method; f) simultaneous method.

By calculating

$$Q = 10\log_{10}\left[\frac{\|m_0\|^2}{\|m_0 - m\|^2}\right],$$

we evaluate and compare the quality and robustness of the frequency band selection strategies, where m_0 and m represent the true velocity model and inverted velocity model, respectively (Anagaw and Sacchi, 2014). A high Q value corresponds to a more accurate solution. The quality factors Q of inverted models for the noisy data in Fig. 14 are shown in Table 3.

Table 3. Quality of the inverted Marmousi velocity model (Q) for noisy data.

Method	Total numbers of forward modeling
Individual-grouping method 1	8,10
Individual-grouping method 2	8,21
Bunks' method	8,22
Partial-overlap grouping method	7,05
Arbitrary-two grouping method	7,09
Simultaneous method	5,47

Table 4 shows the total number of forward modeling simulations in the process of full waveform inversion. Clearly, forward modeling numbers of individual-grouping method 2 are less than those of other efficient methods, which is the least time-consuming method for the high-resolution solution. The above analysis demonstrates that if we use frequency-band selection strategies of individual-grouping method 2 in waveform inversion, satisfactory inverted results can be obtained at a lower computational cost. In particular, we should start from the low frequency components in inversion.

Table 4. Total numbers of forward modelling simulations to achieve final result.

Method	Total numbers of forward modeling
Individual-grouping method 1	9,720
Individual-grouping method 2	9,288
Bunks' method	11,232
Partial-overlap grouping method	10,368
Arbitrary-two grouping method	6,048
Simultaneous method	3,456

CONCLUSIONS

In full waveform inversion, seismic data are more linear in low-frequency bands than in high-frequency bands. If waveform inversion takes advantage of low frequency information, it tends to obtain solutions close to the global minimum even if we start with an inappropriate initial velocity model. Therefore, multiscale method as a feasible selection is proposed to improve the resolution of velocity models.

In this paper, we have introduced three possible frequency-band selection strategies. Individual-grouping method 1 is proposed based on the theory of wavenumber continuity, as the calculated group frequencies have little redundancy in wavenumber information. Individual-grouping method 2 makes use of the relationship between peak frequencies of different scales to calculate the frequency band. Bunks' method starts with low-pass filtered data and then broadens the frequency bands to high frequencies, where the lowest frequencies are fixed for all frequency groups. We examined the effectiveness of the frequency-band selection strategies using tests on Marmousi synthetic data and noisy data. Individual-grouping method 1, Individual-grouping method 2, and Bunks' method all can obtain more satisfactory results than the conventional simultaneous-inversion method, and individual-grouping method 2 performs better in terms of comprehensive factors of resolution, quality and computational cost. The partial-overlap grouping method did not start from zero frequency, and frequency bands had a small amount of overlap, the terrible inversion result implies that low frequencies are an integral part. We also used an arbitrary-two grouping method, whose frequency band is obtained randomly, and inversion falls into local minima.

ACKNOWLEDGEMENTS

This work is supported by the R&D of Key Instruments and Technologies for Deep Resources Prospecting (the National R&D Projects for Key Scientific Instruments), Grant NO. ZDYZ2012-1-06, and Open Issue of Key Laboratory of Mineral Resources, Chinese Academy of Sciences, Grant No. KLMR2015-14.

REFERENCES

Anagaw A.Y. and M. D. Sacchi, 2014. Comparison of multifrequency selection strategies for simultaneous-source full waveform inversion. Geophysics, 79(5): R165-(181. doi: 10.1190/geo2013-0263.1.

Dos Santos, A.W.G. and Pestana, R.C., 2015. Time-domain multiscale full-waveform inversion using the rapid expansion method and efficient step-length estimation. Geophysics, 80(4): R203-R216. doi:10.1190/Geo2014-0338.1.

Berkhout, A.J, 1984. Multidimensional linearized inversion and seismic migration. Geophysics, 49: 1881-1895. doi: 10.1190/1.1441601.

Bérenger, J., 1994. A perfectly matched layer for the absorption of electromagnetic waves. J. Computat. Phys., 114:185-200, doi:10.1006/jcph.1994.1159.

Brenders, A.J. and Pratt, R.G., 2007. Full waveform tomography for lithospheric imaging: Results from a blind test in a realistic crustal model. Geophys. J. Internat., 168: 133-151. doi: 10.1111/j.1365-246X.2006.03156.x.

Bunks, C., Saleck, F.M., Zaleski, S. and Chavent, G., 1995. Multiscale seismic waveform inversion. Geophysics, 60, 1457-1473. doi: 10.1190/1.1443880.

Boonyasiriwat, C., Valasek, P., Routh, P., Cao, W., Schuster, G.T. and Macy, B., 2009. An efficient multiscale method for time-domain waveform tomography. Geophysics, 74(6): WCC59-WCC68. doi: 10.1190/1.3151869.

Brossier, R., Operto, S. and Virieux, J., 2009. Seismic imaging of complex onshore structures by 2D elastic frequency-domain full-waveform inversion. Geophysics, 74(6): WCC105–WCC118. doi: 10.1190/1.3215771.

Biondo, B. and Almomin, A., 2013. Tomographic full-waveform inversion (TFWI) by combining FWI and wave-equation migration velocity analysis. The Leading Edge, 32: 1074-1080, doi: 10.1190/tle32091074.1.

Gauthier, O., Virieux, J. and Tarantola, A., 1986. Two-dimensional nonlinear inversion of seismic waveforms: Numerical results. Geophysics, 51: 1387-1403. doi: 10.1190/1.1442188.

Gao, F., Levander, A., Pratt, R.G., Zelt, C.A., and Fradelizio, G.L., 2007. Waveform tomography at a groundwater contamination site. Surface reflection data. Geophysics, 72(5), G45-G55. doi: 10.1190/1.2752744.

Hager, W.M. and Zhang, H.C.,2006. A survey of nonlinear conjugate gradient methods. Pacif. J. Optimizat., 2: 335–358.

Hu, W.Y., Abubakar, A. and Habashy, T.M., 2009. Simultaneous multifrequency inversion of full-waveform seismic data. Geophysics, 74(2) doi:10.1190/1.3073002.

Ha, W., and Shin, C., 2012. Laplace-domain full-waveform inversion of seismic data lacking low-frequency information. Geophysics, 77(5), doi:10.1190/GEO2011-0411.1.

Kim, Y., Cho, H., Min, D.-J., and Shin, C., 2010. Comparison and frequency-selection strategies for 2D frequency-domain acoustic waveform inversion. Pure Appl. Geophysics, 168, 1715-1727, doi: 10.1007/s00024-010-0196-8.

Lailly. P., 1983. The seismic inverse problems as a sequence of before stack migrations. In: Conf. Inverse Scattering. Theory and Application. Bednar, J.B., Redner, R., Robinson, E. and Weglein, A. (Eds.), Soc. Industr. Appl. Math., Philadelphia. p 206-220.

Liu Y.-S., 2015. Seismic wavefield modeling using the spectral element method and inversion. Ph.D. thesis, University Chinese Academy of Sciences, Beijing.

Liu You-shan, Liu Shao-lin, Zhang Mei-gen et al 2012. An improved perfectly matched layer absorbing boundary condition for second order elastic wave equation. Progress in Geophysics (in Chinese), (5): 2113-2122, doi: 10.6038/j.issn.1004-2903.2012.05.036

Marfurt, K., 1984. Accuracy of finite-difference and finite-elements modeling of the scalar and elastic wave equation. Geophysics, 49: 533–549. doi:10.1190/1.1441689.

Mora, P.R., 1987. Nonlinear two-dimensional elastic inversion of multioffset seismic data. Geophysics, 52: 1211-1228. doi: 10.1190/1.1442384.

Min, D.-J., Shin, J., Shin, C., 2015. Application of the least-squares inversion method: Fourier series versus waveform inversion. Journal of Applied Geophysics, 122, 62-73, doi:10.1016/j.jappgeo.2015.08.006.

Ma, X., Li, Z., Gu, B.-L., Ke, P. and Liang, G.-H., 2015. Comparison and analysis of several optimization finite-differencing schemes in 2D acoustic frequency-domain numerical modeling. Progr. Geophys. (in Chinese), 30: 878-888,. doi: 10.6038/pg20150254.

Nocedal, J. and Wright, S.J., 1999. Numerical Optimization. Springer series in operations research and financial engineering. Springer-Verlag, Berlin.

Nocedal, J., and Wright, S.J., 2006. Numerical Optimization. 2nd edition. Springer-Verlag, Berlin.

Operto, S., Virieux, J., Amestoy, P., L'Excellent, J., Giraud, L., and Ali, H., 2007a. 3D finite-difference frequency-domain modeling of visco-acoustic wave propagation using a massively parallel direct solver: A feasibility study. Geophysics, 72(5): SM195-SM211. doi: 10.1190/1.2759835

Operto, S., Virieux, J., and Sourbier, 2007b. Documentation of FWT2D program (verison 4.8), Frequecy domain full-waveform modeling/inversion of wide-aperture seismic data for imaging 2D acoustic media. Technical report N 007-SESMICCOPE project.

Pratt, R. G., C. Shin, and Hicks, G. J., 1998. Gauss-Newton and full Newton methods in frequency-space seismic waveform inversion. Geophysics, 133: 341-362. doi: 10.1046/j.1365-246X.1998.00498.x.

Pratt, R.G, 1999. Seismic waveform inversion in the frequency domain, Part I: Theory and verification in a physical scale model. Geophysics, 64: 888-901. doi: 10.1190/1.1444597.

Plessix, R., 2006. A review of the adjoin-state method for computing the gradient of a functional with geophysical applications. Geophys. Journal International, 167(2), 495-503, doi: 10.1111/j.1365-246X.2006.02978.x.

Ravaut, C., Operto, S., Improta, L., Virieux, J., Herrero, A., and Aversana, P., 2004. Multiscal imaging of complex structures from multifold wide-aperture seismic data by frequency-domain full waveform tomography. Geophysical J. Internat., 159: 1032-1056. doi: 10.1111/j.1365-246X.2004.02442.x.

Sirgue, L., and Pratt, R. G., 2004. Efficient waveform inversion and imaging: A strategy for selecting temporal frequencies. Geophysics, 69: 231-248. doi: 10.1190/1.1649391.

Shin, C., and Min, D.-J., 2006. Waveform inversion using a logarithmic wavefield. Geophysics, 71(3), R31-R42. doi: 10.1190/1.2194523.

Shin, C., and Cha, Y.-H., 2008. Waveform inversion in the Laplace domain. Geophys. J. Internat., 173: 922-931. doi: 10.1111/j.1365-246X.2008.03768.x.

Symes, W.W., 2008. Migration velocity analysis and waveform inversion. Geophys. Prosp., 56: 765-790. doi: 10.1111/j.1365-2478.2008.00698.x.

Shin, C. and Cha, Y.-H., 2009. Waveform inversion in the Laplace-Fourier domain. Geophys. J. Internat., 177: 1067-1079. doi: 10.1111/j.1365-246X.2009.04102.x.

Tarantola, A., 1984. Inversion of seismic reflection data in the acoustic approximation. Geophysics, 49: 1259-1266. doi: 10.1190/1.1441754.

Vigh, D. and Starr, E.W., 2008. Comparisons for waveform inversion, time domain or frequency domain? Expanded Abstr., 78th Ann. Internat. SEG Mtg., Las Vegas: 1890–1894.

Virieux, J. and Operto, S., 2009. An overview of full-waveform inversion in exploration. Geophysics, 74(6), WCC1-WCC26, doi: 10.1190/1.3238367.

Warner, M., and Guasch, L., 2014. Adaptive waveform inversion: Theory. 84th Annual International Meeting, SEG, Expanded Abstracts, 1089-1093.

Xie, X., 2013. Recover certain low-frequency information for full waveform inversion. Expanded Abstr., 83rd Ann. Internat. SEG Mtg., Houston, 1053–1057.